Water Research 143 (2018) 445–456

Contents lists available at ScienceDirect

Water Research

journal homepage: www.elsevier.com/locate/watres

Evaluation of three turbulence models in predicting the steady state hydrodynamics of a secondary sedimentation tank

Haiwen Gao, M.K. Stenstrom*

Dept. of Civil and Environmental Engineering, University of California Los Angeles, 5714 Boelter Hall, Los Angeles, CA 90095, USA

ARTICLE INFO

Article history:
Received 27 January 2018
Received in revised form
27 June 2018
Accepted 28 June 2018
Available online 29 June 2018

Keywords:
Secondary sedimentation tank
CFD modeling
Standard k-ε
RNG k-ε and realizable k-ε model
Turbulent flow

ABSTRACT

The secondary sedimentation tank (SST) is a sensitive and complicated process in an activated sludge process. Due to the importance of its performance, computational fluid dynamics (CFD) methods have been employed to study the underflow hydrodynamics and solids distribution. Unlike most of the previous numerical studies, in the present investigation, the performance of three different types of turbulence models, standard k-ε, RNG k-ε and Realizable k-ε, are evaluated. Firstly, two-dimensional axisymmetric CFD models of two circular SSTs are validated with the field observations. Next, comprehensive comparisons are presented of the model predictions of the key physical quantities, such as the concentration of effluent suspended solids (ESS), and returned activated sludge (RAS), sludge blanket height (SBH), turbulent properties and flow and concentration patterns.

A surprising result shows that the prediction of the ESS concentration is not sensitive to the change of turbulence models; while remarkable prediction difference can be observed in the inlet zone and near-field of sludge hopper and SBH. The results suggest that more observations inside the inlet zone are needed to achieve better model calibration and correct application of the turbulence model, which can be crucial to optimizing the geometry of inlet structure and sludge hopper as well as changing return solids concentration for the operation.

1. Introduction

Gravity sedimentation is one of the most commonly used treatment methods for removal of suspended solids (SS) in water or wastewater treatment plants. In addition, the cost for building the sedimentation tank is about 30% of the total investment of a treatment plant (Tamayol et al., 2008). For conventional wastewater treatment plants, sedimentation tanks are mainly divided into two categories: primary and secondary sedimentation tanks (SST). Primary sedimentation tanks have a low influent SS concentration; therefore, buoyancy effects are usually negligible. However, SSTs are used to remove and concentrate and recycle biosolids and have much higher influent SS concentrations (Tamayol et al., 2008); therefore, flow currents can be density-driven and affect the performance of SSTs. Ekama and Marais (2002) stated that SSTs are “the bottle neck limiting the capacity of the wastewater treatment plant”. The placement of the two types of the sedimentation tanks is shown in Fig. 1.

Previously, SSTs were designed only using empirical equations, which were based on hydraulic criteria such as surface overflow rate (SOR) (Parker, 1983; Parker and Stenquist, 1986; Parker et al., 1996). Other influential factors such as (1) tank internal geometry, (2) solids characteristics, (3) atmospheric conditions, including wind movement and temperature were not considered (Krebs, 1995; Stamou et al., 2009). Thickening capability was often correlated to the sludge volume index (SVI) but is now usually based upon state-point analysis (Wahlberg and Keinath, 1988).

One-dimensional (1-D) models were developed to estimate solids loading rate and have evolved from conceptual models (Kynch, 1952) to numerical models. The model can solve problems such as the returned activated sludge (RAS) concentration, the sludge blanket height (SBH), and solids inventory management (Kynch, 1952; Takács et al., 1991; Li and Stenstrom, 2014). Although 1-D models are useful in evaluating loads, they cannot include non-ideal effects such as flow currents and poor geometries.

To improve the predicative capability of 1-D models and consider non-ideal conditions, CFD models have been developed over the last 40 years and have improved our knowledge of sedimentation tanks (Larsen, 1977; Zhou and McCorquodale, 1992a,

* Corresponding author.
E-mail address: stenstro@seas.ucla.edu (M.K. Stenstrom).

https://doi.org/10.1016/j.watres.2018.06.067
0043-1354/© 2018 Published by Elsevier Ltd.

Nomenclature

CFD	Computational fluid dynamics
SKE	Standard k-ε model
RNG	Renormalization group k-ε model
RAS	Returned activated sludge
SBH	Sludge blanket height
ESS	Effluent suspended solids
SST	Secondary sedimentation tank
SS	Suspended solids
SOR	Surface overflow rate
1-D	One dimensional
2-D	Two dimensional
3-D	Three dimensional
EDI	Energy dissipated inlet
WWTP	Wastewater treatment plant
TKE	Turbulent kinetic energy
TDR	Turbulent dissipation rate

1992b; 1992c; De Clercq, 2003; Griborio, 2004; Ramin et al., 2014).

The development and the applications of the CFD model of SSTs depend on the following four parts:

(1) Improving the understanding of SSTs by relaxing assumptions for ideal behavior by including physical problems such as the impacts of turbulence and density currents (Larsen, 1977; Adams and Rodi, 1990; Zhou et al., 1992; Wells and LaLiberte, 1998; Jayanti and Narayanan, 2004);
(2) Selecting a mathematical structure for the turbulence and buoyant flow modeling components to more accurately conform to the physical mechanisms (Adams and Rodi, 1990; Bretscher et al., 1992; Vitasovic et al., 1997; Lakehal et al., 1999; Griborio, 2004);
(3) Optimizing the solution to more quickly and accurately solve the differencing equations (Imam and McCorquodale, 1983; Imam et al., 1983; Abdel-Gawad and McCorquodale, 1984a, 1985); (4) Improving computational speed of computers.

Larsen (1977) was among the first to address the physical problems of SSTs and is considered the pioneer in the CFD study of SSTs, setting the framework for the future sedimentation tank research. In his work, the Prandtl mixing length theory was applied to solve the eddy viscosity and was also used in (Abdel-Gawad and McCorquodale, 1984a, 1984b).

The complexity of solving the resulting partial differential equations was reduced with several key assumptions. Constant eddy viscosity was assumed in several early studies (Imam et al., 1983; Krebs, 1991; Krebs et al., 1992, 1995). However, since eddy viscosity depends on the state of turbulence in the SSTs, the value of the eddy viscosity should vary from case to case as well as in different parts of the SSTs. The constant eddy viscosity assumption limited to the accuracy of the models. Additionally, both the mixing length theory model and constant eddy viscosity assumption imply that the turbulence is dissipated where it is generated, which cannot be used to accurately describe the transport of turbulence in the flow field (Griborio, 2004).

Therefore, a more advanced turbulence model (standard k-ε model) which is based on the transport of turbulent kinetic energy (TKE) and the turbulent dissipation rate (TDR) was used to improve many of the previously developed SST models. In the last 30 years, the standard k-ε model (SKE) has become the most widely applied turbulence model in the CFD of SSTs because of its robustness, economy and reasonable accuracy for the prediction of turbulent flow in SSTs (Stamou et al., 1989; Zhou and McCorquodale, 1992b, 1992c; 1992a; Vitasovic et al., 1997; Lakehal et al., 1999; Armbruster et al., 2001; Kleine and Reddy, 2005; Weiss et al., 2007; Tamayol et al., 2009; Gong et al., 2011; Patziger et al., 2012; Xanthos et al., 2013; Ramin et al., 2014).

In the previous studies with circular sedimentation tank, few of velocity and concentration calibrations were reported inside the inlet zone, where the Reynolds number can be very high (turbulent flow). Moreover, the SKE model is valid only for fully turbulent flow and performs poorly for complex flows involving strong streamline curvature (Das et al., 2016; Fluent, 2017). Therefore, two modified versions of the SKE model (RNG k-ε and Realizable k-ε models) have been applied in recent sedimentation tank studies (Laine et al., 1999; Tamayol et al., 2008; Tarpagkou and Pantokratoras, 2013; Patziger and Kiss, 2015; Das et al., 2016). However, in these studies, the RNG k-ε model was applied in the studies of sedimentation tanks either in potable water treatment or primary sedimentation tanks in wastewater treatment, where the buoyancy effect can be ignored in the flow field. To the best of our knowledge, none of the published SSTs papers simulated the density stratified flow with the application of RNG k-ε model. Only Das et al. (2016) has applied the Realizable k-ε model to simulate the turbulent flow in their complex three-dimensional (3D) model, but they had no field observations to show the reliability and superiority of the Realizable k-ε model.

Therefore, because of (1) the limitation of the widely applied SKE model, (2) the superior of the RNG and Realizable k-ε models in predicting the turbulence flow involving strong streamline curvature and (3) the recent applications of the RNG and Realizable k-ε models in the related CFD study areas, these three models are selected to compare their prediction performance in two different SSTs.

In this paper, the influences of the SKE, RNG k-ε and Realizable k-ε models on the performance of a circular SST are compared using data from the Witney wastewater treatment plant (WWTP) from Burt (2010), and the Darvill WWTP from Griborio (2004). Firstly, the computational meshes with different number of cells are applied to ensure the solutions are mesh-independent. Next, the

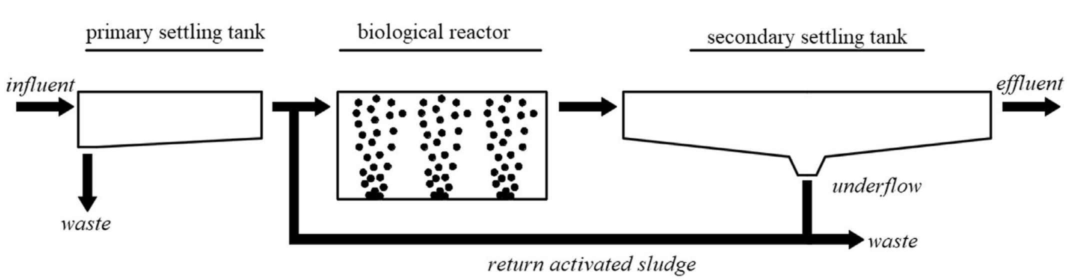

Fig. 1. Layout of a typical AS system (adapted from De Clercq, 2003).

Witney SST simulation results are compared to the measured velocity and concentration profiles. The comparisons show reasonable agreement on the scale of the entire SST. For Darvill only the effluent suspended solids (ESS) concentration and RAS concentrations are available but they also agree well with the simulations. Next the validated models are used with the three different turbulence models to compare the prediction of the hydrodynamics, such as velocity and concentration patterns, especially in the inlet zone and in the near-field zone of the sludge hopper, where significant differences are observed among the three models. Additionally, the predictions of the maximum loading rate by these turbulence models are compared for the Witney SST.

2. Methods

2.1. The mathematical model

2.1.1. General information

Since the dominant hydrodynamics processes of circular SSTs take place in the radial direction, it can reasonably be simplified to a 2-D axisymmetric approach (Zhou and McCorquodale, 1992b; Vitasovic et al., 1997; Lakehal et al., 1999; Griborio, 2004; Tamayol et al., 2009; Patziger et al., 2012; Patziger and Kiss, 2015; Patziger, 2016; Gao and Stenstrom, 2017).

2.1.2. Governing equations

The equations describing 2-D, steady, turbulent, and density stratified flow in a circular SST are as follows:

Continuity equation:

$$\frac{\partial ru}{\partial r}+\frac{\partial rv}{\partial y}=0 \tag{1}$$

r -Momentum component:

$$u\frac{\partial u}{\partial r}+v\frac{\partial u}{\partial y}=-\frac{1}{\rho}\frac{\partial p}{\partial r}+\frac{1}{r}\frac{\partial}{\partial r}\left[r(\vartheta+\vartheta_t)\frac{\partial u}{\partial r}\right]+\frac{1}{r}\frac{\partial}{\partial y}\left[r(\vartheta+\vartheta_t)\frac{\partial u}{\partial y}\right]+S_u \tag{2}$$

y -Momentum component:

$$u\frac{\partial v}{\partial r}+v\frac{\partial v}{\partial y}=-\frac{1}{\rho}\frac{\partial p}{\partial y}+\frac{1}{r}\frac{\partial}{\partial r}\left[r(\vartheta+\vartheta_t)\frac{\partial v}{\partial r}\right]+\frac{1}{r}\frac{\partial}{\partial y}\left[r(\vartheta+\vartheta_t)\frac{\partial v}{\partial y}\right]-g\frac{\rho-\rho_r}{\rho}+S_v \tag{3}$$

where

$$S_u=\frac{1}{r}\frac{\partial}{\partial r}\left[r(\vartheta+\vartheta_t)\frac{\partial u}{\partial r}\right]+\frac{1}{r}\frac{\partial}{\partial y}\left[r(\vartheta+\vartheta_t)\frac{\partial v}{\partial r}\right]-2\frac{\vartheta+\vartheta_t}{r^2}u \tag{4}$$

$$S_v=\frac{1}{r}\frac{\partial}{\partial r}\left[r(\vartheta+\vartheta_t)\frac{\partial u}{\partial y}\right]+\frac{1}{r}\frac{\partial}{\partial y}\left[r(\vartheta+\vartheta_t)\frac{\partial v}{\partial y}\right] \tag{5}$$

u and v are the mean velocity components in the r (radial) and y (axial) directions, respectively. p is the general pressure less the hydrostatic pressure at reference density ρ_r; ρ is the density of mixture, g is the acceleration of gravity, ϑ is the viscosity of the sludge mixture, ϑ_t is the turbulent eddy viscosity. For density-driven flows, the local fluid density is related to the local values of the sediment concentration by the following relationship:

$$\rho=\rho_r+C\left(1-\frac{\rho_r}{\rho_p}\right) \tag{6}$$

in which C is the SS concentration, ρ_p is dry particle density assumed to be 1450 kg/m^3 (Larsen, 1977), ρ_r is reference density (clear water) and ρ is the density of the fluid-solid mixture.

The sludge settling velocity is expressed using the Takács et al. (1991) double exponential function, which is

$$V_s=\max\left(0,\ V_o\left(e^{-r_p(C-C_{min})}-e^{-r_h(C-C_{min})}\right)\right) \tag{7}$$

where V_o is Stokes velocity, r_p and r_h account for rapidly and poorly settling floc, respectively. The constant C_{min} is the concentration of on-settleable solids in the effluent of the SST. The settling parameter values are shown in Table 1.

The solids transport equation in the model is

$$u\frac{\partial C}{\partial r}+v\frac{\partial C}{\partial y}=\frac{1}{r}\frac{\partial}{\partial r}\left[r\left(\vartheta+\frac{\vartheta_t}{\sigma_r}\right)\frac{\partial C}{\partial r}\right]+\frac{1}{r}\frac{\partial}{\partial y}\left[r\left(\vartheta+\frac{\vartheta_t}{\sigma_y}\right)\frac{\partial C}{\partial y}-rV_sC\right] \tag{8}$$

in which C is the concentration of SS, ϑ is the viscosity of the sludge mixture, ϑ_t is the turbulent eddy viscosity, σ_r and σ_y are the turbulent Schmidt numbers in the r and y directions, respectively. Both of them are assumed to be 0.7 in this study. V_s is the sludge settling velocity.

The sludge rheological model is proposed by Bokil (1972):

$$\nu=1\times10^{-6}e^{1.386C}\quad \text{for } C\le 1\text{ g/L}$$

and

$$\nu=2.9\times10^{-6}e^{0.322C}\quad \text{for } C\ge 1\text{g/L} \tag{9}$$

in which C is the concentration of SS.

In Reynolds-averaged Navier Stokes equations, TKE can be calculated based on the turbulence closure method. In this study, three types of turbulence closure approaches (SKE, RNG k-ε and Realizable k-ε models) are applied and compared. The major differences in these models are (1) the turbulent Schmidt numbers governing the turbulent diffusion of TKE and TDR, (2) the source term in the ε and, (3) the method of calculating turbulence (Fluent, 2017).

The standard k-ε model is a semi-empirical model based on the transport equations for the TKE (k) and TDR (ε) (Rodi, 1980). It is assumes that the flow is fully turbulent and the effect of molecular viscosity is negligible (Tamayol et al., 2008). The TKE and TDR are calculated from the following transport equations:

$$u\frac{\partial k}{\partial r}+v\frac{\partial k}{\partial y}=\frac{\partial}{\partial r}\left[\left(\vartheta+\frac{\vartheta_t}{\sigma_k}\right)\frac{\partial k}{\partial r}\right]+\frac{\partial}{\partial y}\left[\left(\vartheta+\frac{\vartheta_t}{\sigma_k}\right)\frac{\partial k}{\partial y}\right]+G_k+G_b-\rho\varepsilon \tag{10}$$

and:

$$u\frac{\partial \varepsilon}{\partial r}+v\frac{\partial \varepsilon}{\partial y}=\frac{\partial}{\partial r}\left[\left(\vartheta+\frac{\vartheta_t}{\sigma_\varepsilon}\right)\frac{\partial \varepsilon}{\partial r}\right]+\frac{\partial}{\partial y}\left[\left(\vartheta+\frac{\vartheta_t}{\sigma_\varepsilon}\right)\frac{\partial \varepsilon}{\partial y}\right]+C_1\frac{\varepsilon}{k}(G_k-C_3G_b)-C_2\rho\frac{\varepsilon^2}{k} \tag{11}$$

Table 1
Loading conditions of the SSTs.

SSTs	Inflow parameters			Settling parameters			Dry solids density
	MLSS	RAS	Q_{inlet}	V_o	r_h	r_p	ρ_p
	g/L	ratio	m^3/d	m/h	L/g	L/g	kg/m^3
Witney	4.187	1.09	4372	12.64	0.340	12.25	1450
Darvill							
Test 1	4.6	0.80	35,986	7.71	0.390	10.00	1450
Test 2	4.3	0.97	32,529	7.71	0.390	10.00	1450
Test 3	3.6	0.79	40,726	7.71	0.390	10.00	1450

G_k represents the generation of TKE due to the mean velocity gradients, and G_b corresponds to the generation of TKE due to buoyancy.

$$G_k = \vartheta_t\left[2\left(\frac{\partial u}{\partial r}\right)^2 + 2\left(\frac{\partial v}{\partial y}\right)^2 + 2\left(\frac{u}{r}\right)^2 + \left(\frac{\partial u}{\partial y} + \frac{\partial v}{\partial r}\right)^2\right] \tag{12}$$

$$G_b = -g\frac{\vartheta_t}{\sigma_t}\frac{\partial \rho}{\partial y} \tag{13}$$

The turbulent viscosity, ϑ_t is then determined as a function of TKE and TDR by

$$\vartheta_t = C_\mu\frac{k^2}{\varepsilon} \tag{14}$$

The dimensionless empirical constants are given the standard values suggested by (Rodi, 1993). $C_\mu = 0.09, C_1 = 1.44, C_2 = 1.92, \sigma_k = 1.0$, and $\sigma_\varepsilon = 1.3$. The value of the empirical constant C_3 related to the buoyancy source term G_b depends on the flow situation (Lakehal et al., 1999). Different researches applied different C_3 values in their specific cases (Lyn et al., 1992; Dahl et al., 1994; Lakehal et al., 1999; Gong et al., 2011; Ramin et al., 2014). Rodi (1993) suggested that C_3 is in the range of 0.8–1.0 for stable stratification that prevails in SSTs and tends toward zero for unstable stratification.

The RNG k-ε model is derived using a statistical technique called the "renormalization group (RNG) theory". The analytical derivation results in a model with constants different from those in the SKE model, and additional terms and functions in the transport equations for TKE and TDR. The RNG k-ε model has a similar form to the SKE model:

$$u\frac{\partial k}{\partial r} + v\frac{\partial k}{\partial y} = \frac{\partial}{\partial r}\left(\alpha_k\mu_{eff}\frac{\partial k}{\partial r}\right) + \frac{\partial}{\partial y}\left(\alpha_k\mu_{eff}\frac{\partial k}{\partial y}\right) + G_k + G_b - \rho\varepsilon \tag{15}$$

and:

$$u\frac{\partial \varepsilon}{\partial r} + v\frac{\partial \varepsilon}{\partial y} = \frac{\partial}{\partial r}\left(\alpha_\varepsilon\mu_{eff}\frac{\partial \varepsilon}{\partial r}\right) + \frac{\partial}{\partial y}\left(\alpha_\varepsilon\mu_{eff}\frac{\partial \varepsilon}{\partial y}\right) + C_1\frac{\varepsilon}{k}(G_k - C_3G_b) - C_2\rho\frac{\varepsilon^2}{k} - R_\varepsilon \tag{16}$$

In these equations, G_k and G_b are the same as in the SKE model. The quantities α_k and α_ε are the inverse effective Prandtl numbers:

$$\left|\frac{\alpha - 1.3929}{\alpha_o - 1.3929}\right|^{0.6321}\left|\frac{\alpha + 2.3929}{\alpha_o + 2.3929}\right|^{0.3679} = \frac{\mu_{mol}}{\mu_{eff}} \tag{17}$$

where $\alpha_o = 1.0$.

The main difference between RNG and SKE models appears in the additional term R_ε in the TDR equation, which is more responsive to the effects of rapid strain and streamline curvature than the SKE model and may have a superior performance in the simulation of sedimentation tank model with a complex inlet geometry. The definition of the R_ε and its effects on the prediction of the TDR are illustrated in the ANSYS Fluent Theory Guide, equations 4.48 to 4.50 (Fluent, 2017). The dimensionless model constants are:

$C_1 = 1.42$, $C_2 = 1.68$

Another modified k-ε model is the Realizable k-ε model. It involves a modified transport equation for the TDR, which has been derived from an exact equation for the transport of the mean-square vorticity fluctuation. Compared with SKE, Realizable k-ε model gives a much more accurate prediction of Reynolds stresses for flow with rotation and recirculation (Das et al., 2016). The modeled transport equations for TKE and TDR in the Realizable k-ε model are

$$u\frac{\partial k}{\partial r} + v\frac{\partial k}{\partial y} = \frac{\partial}{\partial r}\left[\left(\vartheta + \frac{\vartheta_t}{\sigma_k}\right)\frac{\partial k}{\partial r}\right] + \frac{\partial}{\partial y}\left[\left(\vartheta + \frac{\vartheta_t}{\sigma_k}\right)\frac{\partial k}{\partial y}\right] + G_k + G_b - \rho\varepsilon \tag{18}$$

and:

$$u\frac{\partial \varepsilon}{\partial r} + v\frac{\partial \varepsilon}{\partial y} = \frac{\partial}{\partial r}\left[\left(\vartheta + \frac{\vartheta_t}{\sigma_\varepsilon}\right)\frac{\partial \varepsilon}{\partial r}\right] + \frac{\partial}{\partial y}\left[\left(\vartheta + \frac{\vartheta_t}{\sigma_\varepsilon}\right)\frac{\partial \varepsilon}{\partial y}\right] - C_1\frac{\varepsilon}{k}C_3G_b + \rho C_1S\varepsilon - \rho C_2\frac{\varepsilon^2}{k + \sqrt{\vartheta\varepsilon}} \tag{19}$$

where

$$C_1 = \max\left[0.43,\ \frac{\eta}{\eta + 5}\right],\ \eta = \frac{Sk}{\varepsilon} \tag{20}$$

The turbulent viscosity has the same form as in SKE model:

$$\vartheta_t = C_\mu\frac{k^2}{\varepsilon} \tag{21}$$

However, C_μ is no longer constant and is a function of the mean strain and rotation rates, the angular velocity of the system rotation, and the turbulent fields.

2.1.3. Boundary conditions

Velocity inlet boundary condition is applied to inlet and sludge bottom boundaries, which assumes a uniform distribution of all the dependent variables at the boundary face. For the surface outlet, a pressure outlet boundary condition is applied, which assumes a uniform pressure and zero-gradient for all transport variables. Instead of estimating the TKE and TDR, turbulent intensity and hydraulic diameter are used as the turbulence specification method on the inlet and outlet boundaries. For the free ambient water surface, the rigid-lid approximation for all velocity components with full slip shear condition is assumed (Wang et al., 2008; Tarpagkou and Pantokratoras, 2013). And the free surface boundary is treated as a symmetry condition. The solid boundaries are specified as stationary walls with a no slip-shear condition and standard wall function is used with the turbulence models.

2.1.4. Solution procedure

The governing equations are numerically solved by the commercial CFD code ANSYS Fluent v.17.2. A first-order upwind method is used for interpolation of variables to cell faces for the convective terms, whereas diffusive terms are discretized using second order central differencing. Pressure-velocity coupling is achieved using the SIMPLE method.

The solution procedures which are accomplished in meshes with different grid numbers can be summarized in the following steps:

(1) The flow filed with pure water is firstly solved in the absence of turbulence. Convergence is reached when normalized residuals are less than 10^{-4};
(2) The converged solution is interpolated into the pure water flow field, coupled with SKE model to calculate the steady state turbulence flow field. None of the buoyancy damping terms to the TKE and TDR are included. Convergence is reached when normalized residuals are less than 10^{-4};
(3) The solids transport equation defined in the User Define Scalar is coupled to the model;
(4) The buoyancy damping term (G_b) is included to the TKE equation to describe the turbulent and density stratified flow;
(5) The buoyancy damping term (G_b) associated with C_3 is added to the TDR equation to complete the procedure.

In the steps 3 to 5, convergence is achieved when the following three criteria are all achieved:

(1) Normalized residuals are less than 10^{-3} or the solution no longer changes with subsequent iterations;
(2) The net flux imbalance is less than 1% of the smallest flux through the domain boundary;
(3) Other monitored key physical quantities no longer change with subsequent iterations.

The velocity profiles as a function of depth for Witney and Darvill SSTs, are calculated from meshes with different grid numbers at three radial locations, and are shown in the supplementary material (Figs. S1 and S2, respectively). After achieving grid independence tests, the second-order upwind method is used to calculate a more accurate solution for the final step described in the previous solution procedures.

2.2. Geometry and meshing

The geometries and meshes are generated using Ansys Meshing v.17.2. The general geometry of the Witney SST with the computational mesh (Fine mesh) that is used in the simulations after achieving grid independent test consists of 428,000 cells. In order to ensure that the solution is mesh-independent, three additional meshes are used, one coarse consisting of 123,096 cells, a medium one consisting of 225,284 cells and a finer one consisting of 901,136 cells. Fig. S1 shows that the difference between the prediction of the coarse mesh to other three finer (medium, fine and finer) meshes is significant, but the difference among the prediction of the three finer meshes is negligible. Therefore, the solution from the mesh of 428,000 cells is considered mesh-independent.

The general geometry of the Darvill SST with the computational mesh that is used in the simulations after achieving grid independent test consists of 218,700 cells. In order to ensure that the solution is mesh-independent, two additional finer meshes are used, one consisting of 389,428 cells and another one consisting of 874,800 cells. Fig. S2 shows that the difference among the prediction of these three meshes is negligible. Therefore, the solution from the mesh of 218,700 cells is considered mesh-independent and has the benefit of increased computational speed.

The general geometry of the Witney and Darvill SSTs are displayed in Figs. 2 and 3, respectively. Since the outlet is extremely small compared with inlet, the grids near the outlet zone are enlarged to show the outlet boundary condition clearly. The dimensions of the Witney and Darvill SSTs are shown in Table 2.

2.3. Model verification

Since only the measurements of the velocity and concentration profiles for the Witney SST are available in Burt (2010), they are used to compare the model predictions for the Witney SST. The comparisons of the velocity and concentration profiles along the SST radial direction between the model predictions and the field measurements are shown in Figs. 4 and 5, respectively. However, the predictions of Darvill SST are compared with the observed performance indicators, such as ESS and RAS concentrations, of three tests in Ekama and Marais (2002) and Griborio (2004). The investigated loading conditions for Witney and Darvill SSTs are shown in Table 1.

Figs. 4 and 5 show the velocity and concentration profiles comparison along the radial direction of Witney SST between the model predictions and the field measurements, respectively. In Fig. 4, the overall stream curvatures outside of the stilling well are reasonably predicted, but less well predicted inside the stilling well. Fig. 5 indicates that the predictions of the bed transition (0.85 g/L contour followed by Burt (2010)) agree reasonably well with the measurements, but sludge blanket concentration is less well predicted.

3. Results and discussions

3.1. Performance indicators

Comparisons among the predictions of the performance indicators by the different turbulence models and the field data in Darvill and Witney SSTs are shown in Figs. 6 and 7, respectively. Figs. 6 and 7 show that the predictions of ESS by the three models are quite similar. All the models show fair agreement with the field data of the Darvill SST and show good agreement with the field data of the Witney SST.

For the RAS concentration, Fig. 6 shows that all the turbulence models give a similar prediction of RAS concentration and show reasonable agreement with the field data in Tests 2 and 3. However, in the Test 1, Realizable k-ε model gives a 10% higher of RAS concentration prediction than the SKE model. Additionally, the difference among the prediction of RAS concentration for the Witney SST is also significant as shown in Fig. 7.

The predictions of SBH by the three turbulence models for the Darvill SST are also varied. The largest prediction difference is shown in Test 3, where the Realizable k-ε produces a 14.1% lower SBH than the prediction by SKE.

The predicted RAS concentration in the local area of inlet zone, as shown in Figs. 6 and 7, and the SBH in Fig. 6, show remarkable

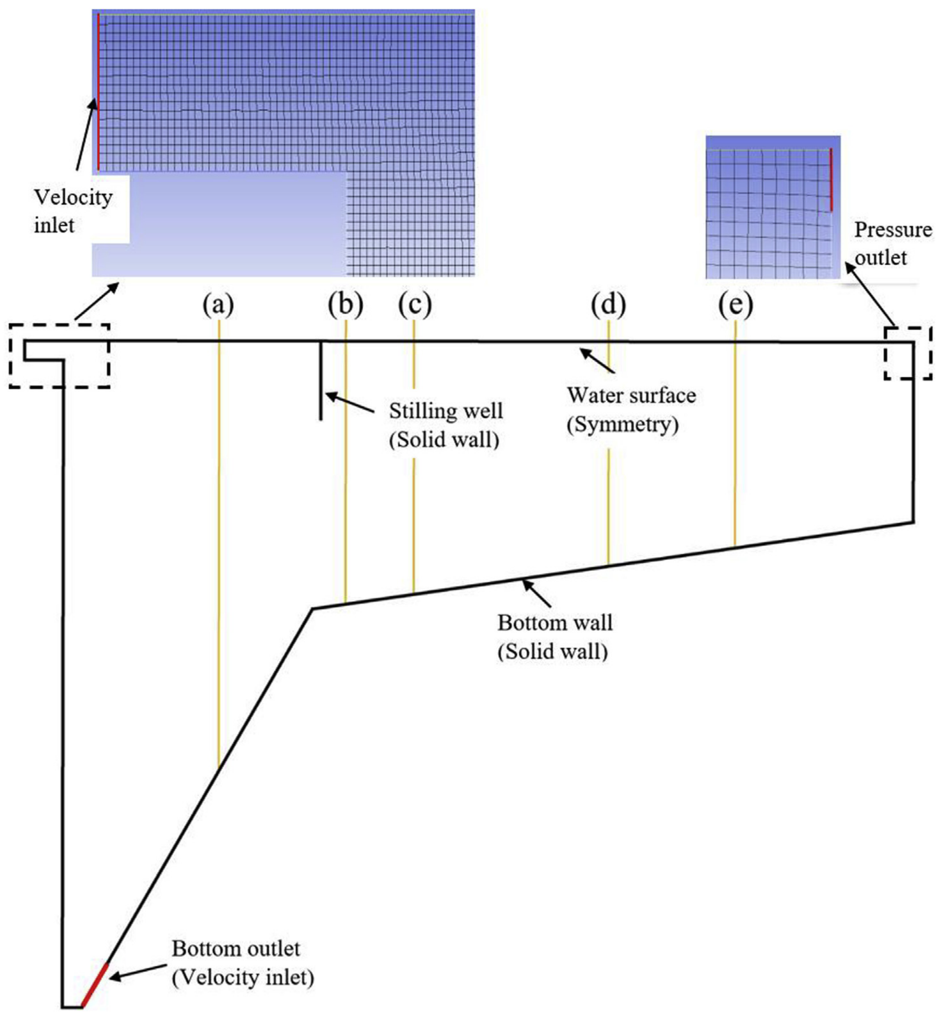

Fig. 2. Witney SST Diagrams with representative computed locations and boundary conditions. (a)–(e) refer to the radial locations for the grid independent tests shown in Fig. S1 and model verification shown in Figs. 4 and 5.

disagreement, indicating that the influence of turbulence is important.

3.2. Velocity and concentration contours for Darvill SST

Fig. 8(a–c) presents the predictions of the velocity magnitude vectors in the inlet zone and concentration contours by the SKE (a), RNG k-ε (b) and Realizable k-ε (c) models for the Test 1 of Darvill SST, respectively. It shows that the predicted turbulent flow contours by the SKE and RNG k-ε models are similar. Both models show the influent flows into the center well immediately turns sharply downward without impinging the baffle, and then changes its direction towards the baffle in the near-field zone above the sludge hopper and finally flows as a horizontal jet from the bottom lip of the baffle outside the inlet zone. Additionally, both SKE (a) and RNG k-ε (b) models predict the formation of a small eddy below the inlet port and a large eddy between the downward jet and baffle, from the surface to the turning point of jet at the bottom.

However, the flow contour predicted by Realizable k-ε inside the inlet zone is totally different from the simulation result using SKE and RNG k-ε turbulence models. The Realizable k-ε model predicts that the horizontal inflow jet impinges on the center of the baffle and is then forced in the opposite direction before reversing directions to form a horizontal jet from the lip of the baffle outside the inlet zone. Additionally, Realizable k-ε (c) predicts a larger eddy below the inlet port and a compressed eddy in the triangulated area bounded by the surface, baffle and downward jet. Moreover, the region of the high downward flow (shown as red in Fig. 8a and b) predicted by the Realizable k-ε is much smaller than the region predicted by the other two models.

The prediction of the magnitude and the location of the peak velocity is also different. Results of the Realizable k-ε also show that the location of the peak velocity (0.131 m/s) is at the inlet port, while both SKE (0.149 m/s) and RNG k-ε (0.183 m/s) models predict it is at the center of the core of the high downward flow.

Fig. 9 presents the quantitative comparisons of the velocity magnitude of the three models inside and outside the inlet zone for Test 1 of Darvill SST. Consistent with the qualitatively comparisons in Fig. 8, SKE and RNG k-ε models have similar velocity magnitude distribution from the surface to bottom, although the peak velocity prediction and the vertical position of the peak velocity have some small differences. However, large disagreement of the velocity magnitude distribution can be found between Realizable k-ε and SKE/RNG k-ε in the inlet zone. Outside of the inlet zone, the difference reduces gradually along the radial direction as the energy is dissipated.

The flow contours predicted by the SKE and RNG k-ε models are similar which creates similar concentration profiles. In both cases

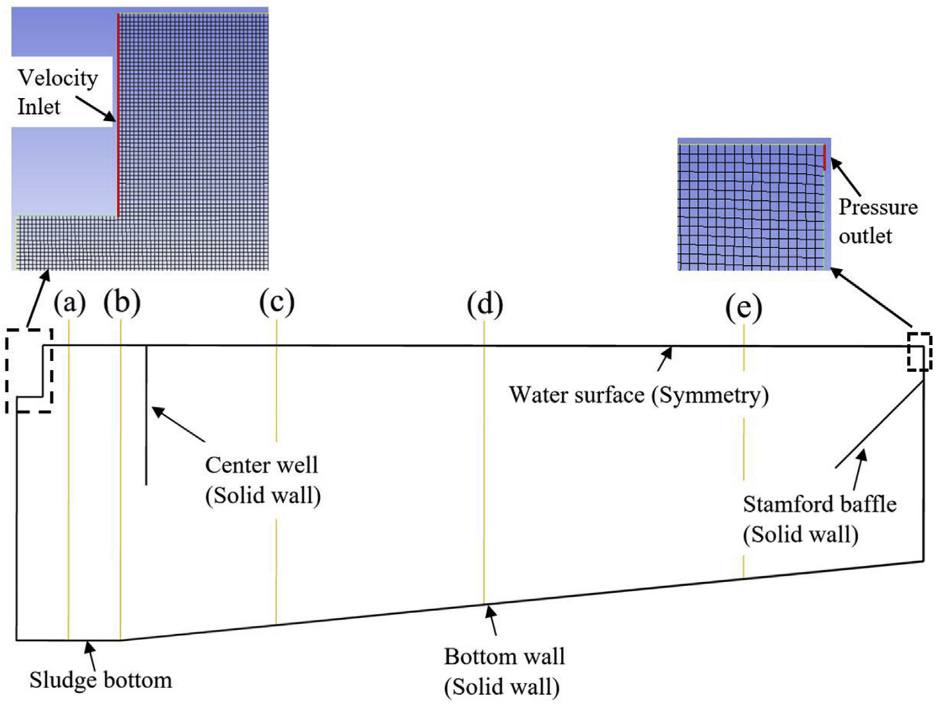

Fig. 3. Darvill SST Diagrams with representative computed locations and boundary conditions. (a)–(e) refer to the radial locations for the grid independent tests shown in Fig. S2 and model comparisons shown in Fig. 9.

Table 2
Dimensions of SSTs.

Geometry	Values	
	Witney	Darvill
Diameter of the clarifier	18.3 m	35.0 m
Surface area	263 m^2	962 m^2
Radius of the inlet pipe	0.4 m	0.5 m
Depth of side wall	1.8 m	4.1 m
Tank floor slope	7.5%	10%
Hopper floor slope	60°	/
Stilling/Center well diameter	5.49 m	6.0 m
Stilling/Center well depth	0.8 m	2.7 m
Stamford baffle depth	/	0.6 m
Stamford baffle length	/	1.7 m
Outboard launder	Peripheral launder	Peripheral launder

the concentrations in inlet, outlet, main settling and bottom sludge zones and the SBH are all similar. However, the velocity and concentration predictions of SKE and RNG k-ε models of the sludge in the near-field zone of the sludge hopper are quite different than predicted by the Realizable k-ε model. The differences in concentrations predicted by the Realizable k-ε are caused by the high downward velocities inside the center well, as shown in Fig. 8c. The magnitude and pattern of the velocities near the middle of the center well are quite different. The downward velocity predicted by the Realizable k-ε model at R = 1.0 m is lower and does not closely approach the sludge hopper, as observed in the SKE and RNG k-ε results. Fig. 8 shows that the concentration above the sludge hopper ranges from 4 to 11 g/L (green to red) for the SKE and RNG k-ε model results, while the Realizable k-ε predictions for

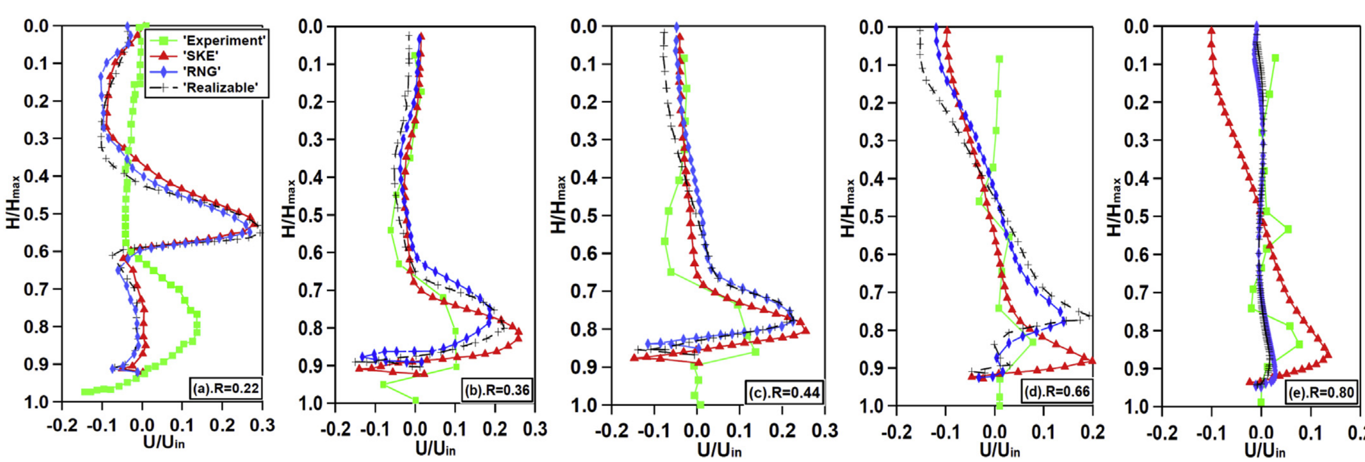

Fig. 4. Comparison of radial velocity profiles by various turbulence models with field measurements for Witney SST. R is the ratio between the radial distance of the vertical measurement location to the radius of tank.

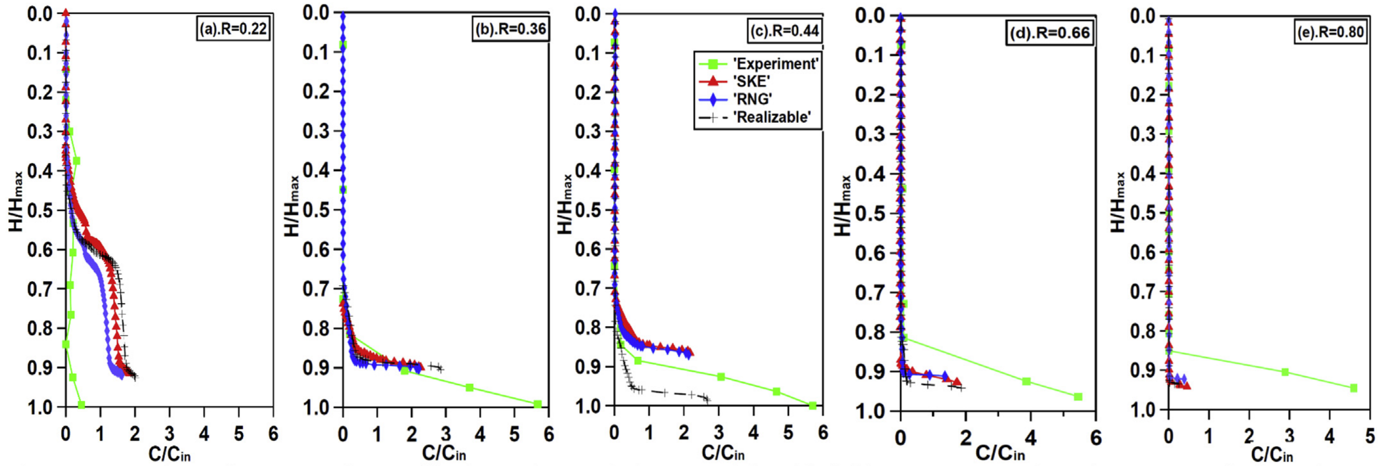

Fig. 5. Comparison of concentration profiles by various turbulence models with field measurements for Witney SST. R is the ratio between the radial distance of the vertical measurement location to the radius of tank.

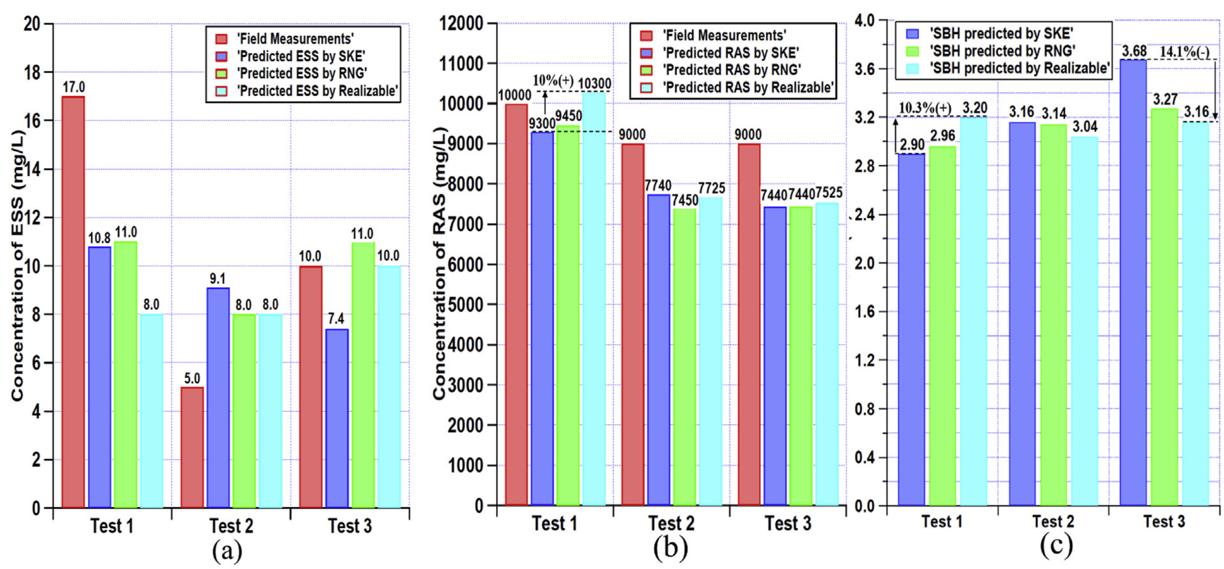

Fig. 6. Comparison among the predictions of the performance indicators with SKE, RNG k-ε, Realizable k-ε turbulence models and field data for Darvill SST.

concentrations in this area range from 8 to 11 g/L (yellow-orange to red).

The Realizable k-ε model results show a similarity of the overall concentration contour within the SST but produces a more homogeneous, highly concentrated sludge blanket in the near-field zone of the sludge hopper and a shallower sludge blanket (Fig. 8c), as compared to the SKE and RNG k-ε results. This is because the high downward flow predicted by SKE and RNG k-ε in the inlet zone swirls up the settled sludge, which results in drifting of the settled sludge particles and insufficient transport towards sludge hopper (Patziger et al., 2016); therefore, elevating the entire sludge blanket.

3.3. Velocity contour for Witney SST

Fig. 10 indicates that these three turbulence models predict the similar flow contour on the scale of the entire Witney SST; therefore, the similar concentration contour. All the models predict that the inflow turns sharply downward as a density current without reaching the stilling well. However, the SKE model predicts a 15.8% longer length of the bottom horizontal jet flow than the prediction of the RNG and Realizable k-ε models, which indicates the SKE model predicts a stronger horizontal jet than the prediction of the RNG and Realizable k-ε models. Also, Fig. 4b-e shows the prediction of the bottom horizontal jet by SKE model is deeper and closer to the sludge blanket surface. Since the strong and deep horizontal flow jet can easily drift and swirl up the settled sludge (Patziger, 2016), the SKE model predicts a higher ESS than the prediction of the RNG and Realizable k-ε models (shown in Fig. 7a). As the increase of the influent rate, the SKE model may predict the failure of SST when the RNG and Realizable k-ε models still predict the well-operated SST.

3.4. CFD stress tests for the Witney SST

3.4.1. Predictions of the flow capacity

In order to compare the prediction of the Witney SST capacity by these turbulence models, stress tests are simulated by increasing the influent rate. The failure of the SST is accepted as ESS>30 mg/L. MLSS and RAS ratio keep constant. Fig. 11 shows the prediction of the ESS under the original influent rate and the

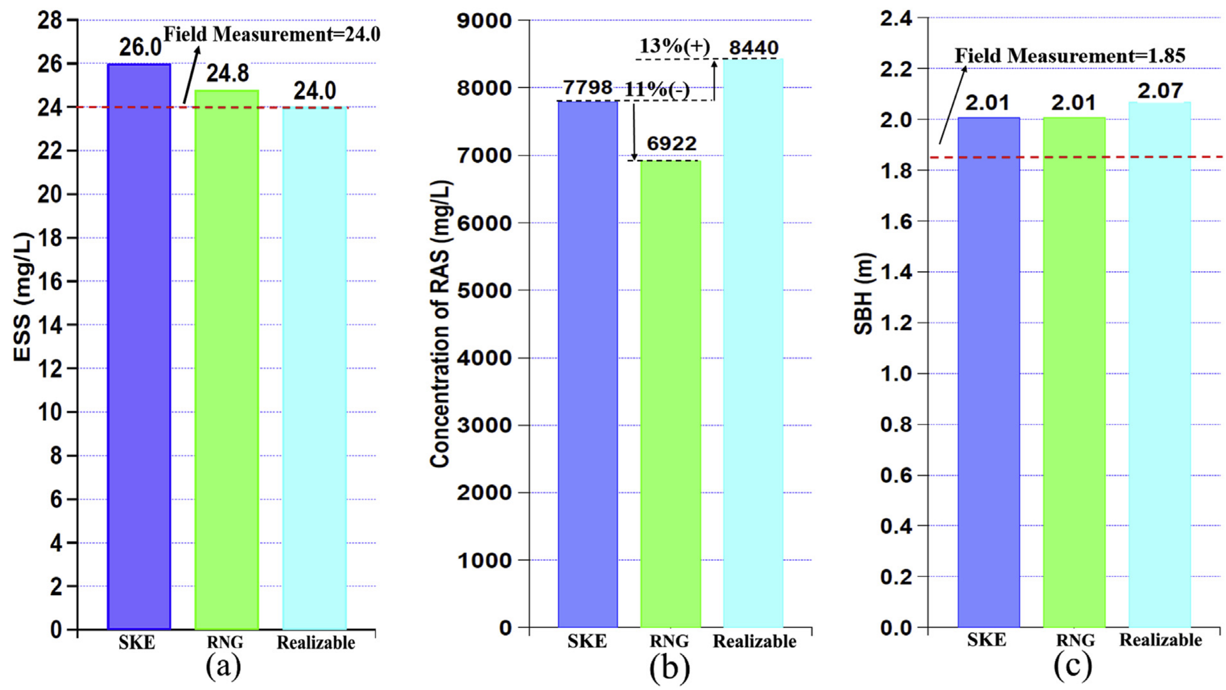

Fig. 7. Comparison among the predictions of the performance indicators with SKE, RNG k-ε, Realizable k-ε turbulence models and field data for Witney SST.

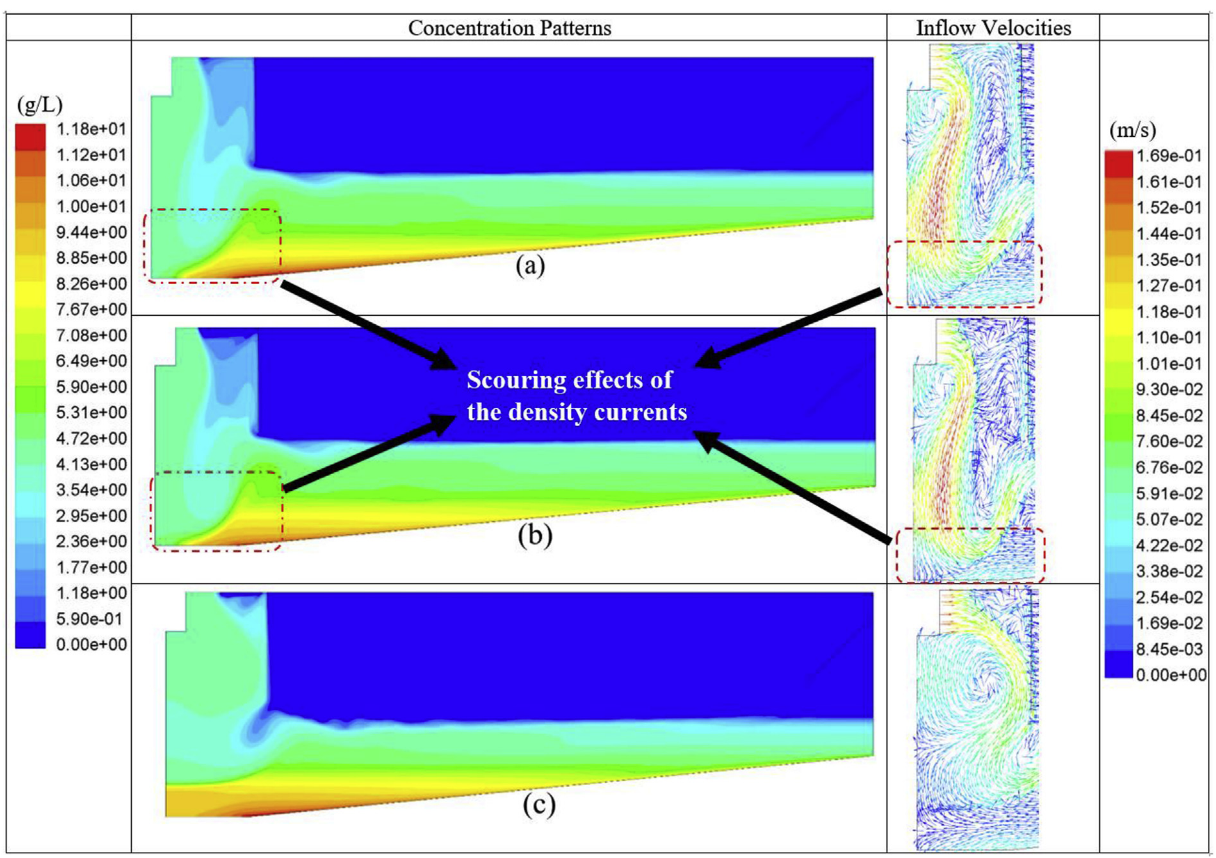

Fig. 8. Flow and concentration contours for the Test 1 of Darvill SST predicted by (a) SKE, (b) RNG k-ε and (c) Realizable k-ε turbulence models.

limiting influent rate by these turbulence models. The limiting influent rate (or the maximum loading rate) predicted by the SKE model is 6120 m^3/d (surface overflow rate, SOR = 0.464 m/h) when ESS reaches 30 mg/L, while the predictions of the limiting influent rates are 6630 (SOR = 0.502 m/h) and 8026 m^3/d (SOR = 0.608 m/h), respectively, by the RNG and Realizable k-ε

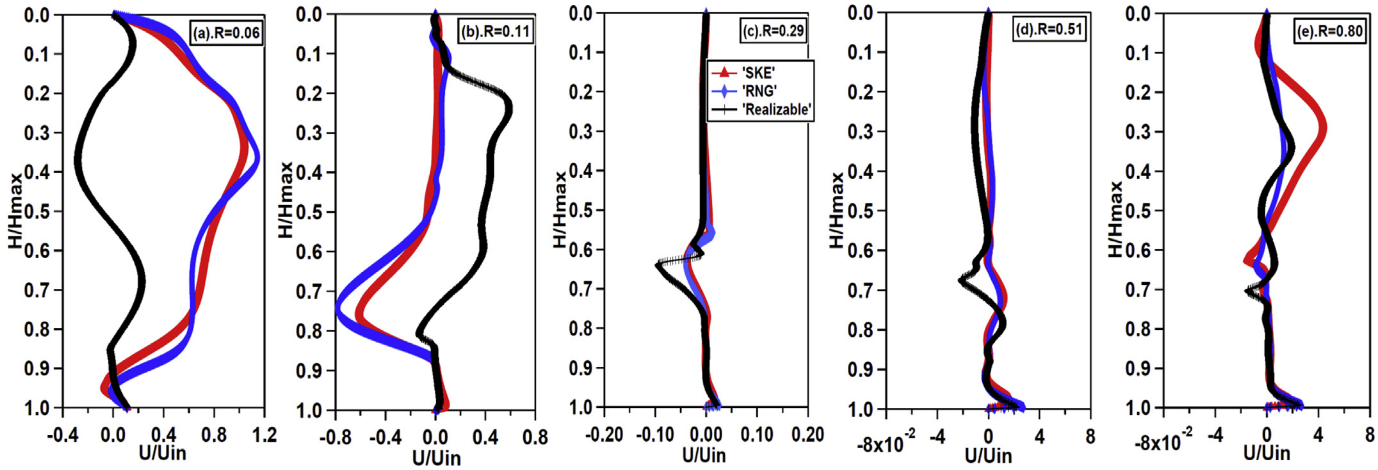

Fig. 9. Comparison among the predictions of radial velocity profiles (m/s) by various turbulence models for the Test 1 of Darvill SST. R is the ratio between the radial distance of the vertical measurement location to the radius of tank.

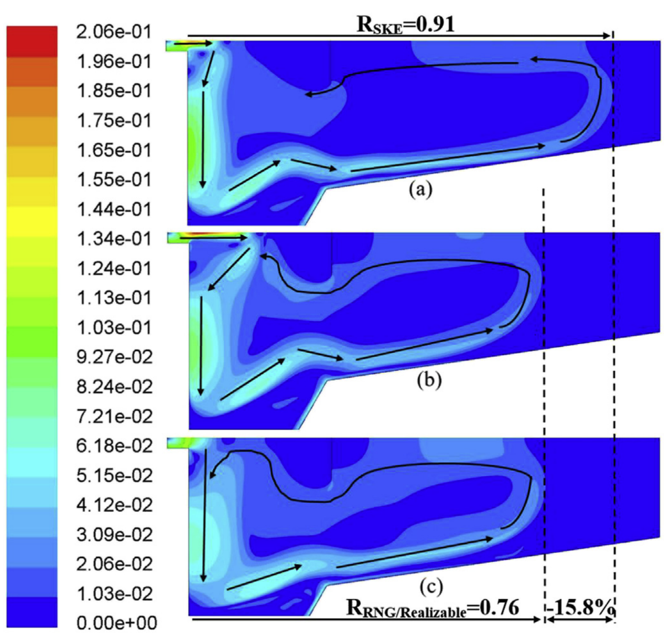

Fig. 10. Predictions of flow patterns (m/s) for the Witney SST by the turbulence models: (a) SKE model, (b) RNG model, (c) Realizable *k-ε* model.

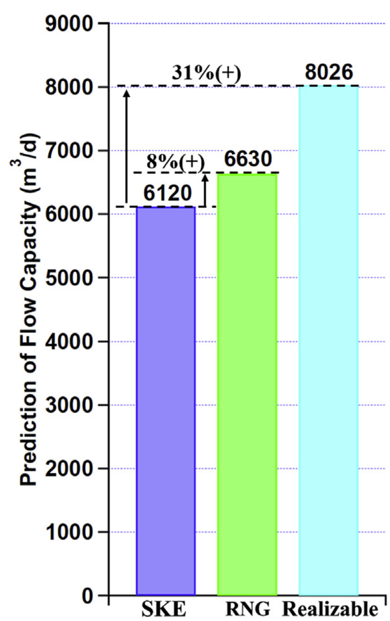

Fig. 11. Prediction of the flow capacity by the SKE, RNG and Realizable *k-ε* turbulence models.

models. The limiting influent rates predicted by the RNG and Realizable *k-ε* models are about 8% and 31% higher than predicted by the SKE model, respectively. This indicates that the turbulence model selection strongly influences the prediction of the Witney SST's flow capacity.

3.4.2. Comparison of the predicted velocity contours under the maximum loading rate

Fig. 12 shows the prediction of the velocity contours by these turbulence models when their prediction of the ESS reaches 30 mg/L. The RNG model does not predict the downward density current that the other two models predict as shown in Fig. 10. At lower loading rates, simulations with all three models predict similar flow contours. In Fig. 12, the SKE and Realizable *k-ε* models similarly predict the density currents from the inlet without reaching the stilling well, while the RNG model predicts a strong horizontal jet impinging on the baffle.

Based on the similarity and difference predicted by these turbulence models under the original and maximum loading rates, especially in the inlet zone, Table 3 shows a diagnostic approach to select the most accurate turbulence model. The same symbol in a column indicates that the predictions of the turbulence models are similar. The first column indicates that the predictions of the velocity and concentration fields by these turbulence models are all similar under the original loading rate and one cannot decide the most accurate turbulence model. Next, the second column shows that the predictions of the flow capacity by the SKE model are significantly different from the RNG and Realizable *k-ε* models. If the experimental data show the actual maximum flow capacity is close to the prediction of the SKE model, the SKE model is the optimal turbulence model. Otherwise, the velocity and concentration profiles under the maximum loading rate, especially in the inlet zone, need to be measured to select the optimal model from the RNG and Realizable *k-ε* models.

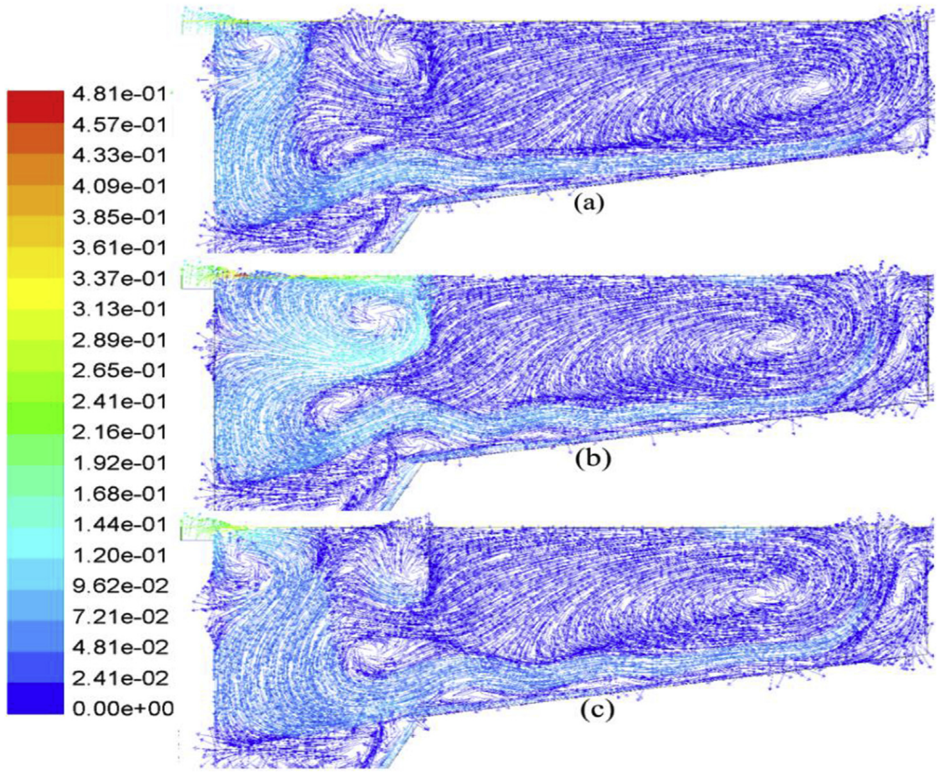

Fig. 12. Comparison of the predicted flow contours (m/s) for the Witney SST under the maximum hydraulic loading condition: (a) SKE model, (b) RNG model, (c) Realizable k-ε model.

Table 3
Prediction similarity and difference by these turbulence models under the original and maximum loading rates.

	Velocity and concentration profiles under the original loading rate	Flow capacity	Velocity and concentration profiles under the maximum loading rate
SKE	+	-	+
RNG	+	+	-
Realizable	+	+	+

Same symbol in a column indicates the prediction similarity by these turbulence model.

4. Conclusions

In this paper, a Fluent-based 2D axisymmetric numerical model is used to analyze the hydrodynamics and turbulent flow, such as flow and concentration patterns of two different SSTs. The previous numerical studies did not study the effect of different turbulent models on the turbulent flow and concentration pattern in the inlet zone, where they can have major impacts. In the present work numerical simulations with three advanced turbulent models (SKE, RNG k-ε and Realizable k-ε) are performed on two different SSTs to study the influence of turbulent models on the flow and concentration patterns and operation parameters, such as ESS, RAS concentration and SBH. Also, the predictions of the SST capacity are compared using the three turbulence models.

For the case studied by various turbulence models, the following conclusions are made:

- Turbulence model selection can have a strong influence on the prediction of hydrodynamics of an SST, such as flow and concentration patterns. The difference is remarkable inside the inlet zone, where the high flow energy is dissipated, resulting in high turbulence.
- The remarkable different predictions of the hydrodynamics inside the inlet zone cause significant differences (more than 10%) in predicting RAS concentration and SBH, which can greatly influence the operation of sludge return concentration.
- Turbulence model selection also can have a strong influence on the prediction of flow capacity. The RNG and Realizable k-ε models predict 8% and 31% higher of the flow capacity than the SKE model, respectively, for the Witney SST.
- The significant difference among the predictions of the turbulence models inside the inlet zone of Darvill SST under the original loading rate and of Witney SST under the maximum loading rate suggest that more observations are required in this area for model verification and turbulence model selection.

The turbulence models as shown with these simple geometries have a strong influence on the prediction of the SST hydrodynamics inside the inlet zone. For geometries with complex inlet baffling structures, such as the LA or tangential energy dissipating inlet structure which cannot be easily simplified to a 2-D axisymmetric mesh, it is especially necessarily to study the influence of the turbulence model. Such complex geometries use will likely require 3-D meshes to better predict SST performance, and turbulence model selection should have a major impact.

Future work should include non-steady state simulations to better understand the hydrodynamics predicted by these turbulence models during transient conditions. Other advanced turbulence models, such as the large eddy simulation model by Al-Sammarraee et al. (2009), should also be considered in the future turbulence model comparisons.

Appendix A. Supplementary data

Supplementary data related to this article can be found at https://doi.org/10.1016/j.watres.2018.06.067.

References

Abdel-Gawad, S., McCorquodale, J., 1985. Numerical simulation of rectangular settling tanks. J. Hydraul. Res. 23 (2), 85–100.
Abdel-Gawad, S.M., McCorquodale, J.A., 1984a. Hydrodynamic of circular primary clarifiers. Can. J. Civ. Eng. 11 (2), 299–307.
Abdel-Gawad, S.M., McCorquodale, J.A., 1984b. Strip integral method applied to settling tanks. J. Hydraul. Eng. 110 (1), 1–17.
Adams, E.W., Rodi, W., 1990. Modeling flow and mixing in sedimentation tanks. J. Hydraul. Eng. 116 (7), 895–913.
Al-Sammarraee, M., Chan, A., Salim, S.M., Mahabaleswar, U.S., 2009. Large-eddy simulations of particle sedimentation in a longitudinal sedimentation basin of a water treatment plant. Part I: particle settling performance. J. Chem. Eng. 152, 315–321.
Armbruster, M., Krebs, P., Rodi, W., 2001. Numerical modelling of dynamic sludge blanket behaviour in secondary clarifiers. Water Sci. Technol. 43 (11), 173–180.
Bretscher, U., Krebs, P., Hager, W.H., 1992. Improvement of flow in final settling tanks. J. Environ. Eng. 118 (3), 307–321.
Bokil, S.D., 1972. Effect of Mechanical Blending on the Aerobic Digestion of the Waste Activated Sludge. Ph.D. thesis. Department of Civil and Engineering, University of Windsor, Ontario, Canada.
Burt, D.J., 2010. Improved Design of Settling Tanks Using an Extended Drift Flux Model. Ph.D. thesis. University of Bristol, UK.
Dahl, C., Larsen, T., Petersen, O., 1994. Numerical modelling and measurement in a test secondary settling tank. Water Sci. Technol. 30 (2), 219–228.
Das, S., Bai, H., Wu, C., Kao, J.-H., Barney, B., Kidd, M., Kuettel, M., 2016. Improving the performance of industrial clarifiers using three-dimensional computational fluid dynamics. Eng. Appl. Comp. Fluid 10 (1), 130–144.
De Clercq, B., 2003. Computational Fluid Dynamics of Settling Tanks: Development of Experiments and Rheological, Settling, and Scraper Submodels. BIOMATH. University of Ghent, Ghent.
Ekama, G., Marais, P., 2002. Hydrodynamic Modelling of Secondary Settling Tanks. WRC Rep. No. 835/1/02 Part 1.
Fluent, A., 2017. ANSYS Fluent 18.0 Theory Guide.
Gao, H., Stenstrom, M.K., 2017. Computational Fluid Dynamics Applied to Secondary Clarifier Analysis, pp. 301–315.
Gong, M., Xanthos, S., Ramalingam, K., Fillos, J., Beckmann, K., Deur, A., McCorquodale, J.A., 2011. Development of a flocculation sub-model for a 3-D CFD model based on rectangular settling tanks. Water Sci. Technol. 63 (2), 213–219.
Griborio, A., 2004. Secondary Clarifier Modeling: a Multi-process Approach. Ph.D. thesis. UNO.
Imam, E., McCorquodale, J.A., 1983. Simulation of flow in rectangular clarifiers. J. Environ. Eng. 109 (3), 713–730.
Imam, E., McCorquodale, J.A., Bewtra, J.K., 1983. Numerical modeling of sedimentation tanks. J. Hydraul. Eng. 109 (12), 1740–1754.
Jayanti, S., Narayanan, S., 2004. Computational study of particle-eddy interaction in sedimentation tanks. J. Environ. Eng. 130 (1), 37–49.
Kleine, D., Reddy, B.D., 2005. Finite element analysis of flows in secondary settling tanks. Int. J. Numer. Method. Biomed. Eng 64 (7), 849–876.
Krebs, P., 1991. The hydraulics of final settling tanks. Water Sci. Technol. 23 (4–6), 1037–1046.
Krebs, P., 1995. Success and shortcomings of clarifier modelling. Water Sci. Technol. 31 (2), 181–191.
Krebs, P., Vischer, D., Gujer, W., 1992. Improvement of secondary clarifiers efficiency by porous walls. Water Sci. Technol. 26 (5–6), 1147–1156.
Krebs, P., Vischer, D., Gujer, W., 1995. Inlet-structure design for final clarifiers. J. Environ. Eng. 121 (8), 558–564.
Kynch, G.J., 1952. A theory of sedimentation. Trans. Faraday Soc. 48, 166–176.
Laine, S., Phan, L., Pellarin, P., Robert, P., 1999. Operating diagnostics on a flocculator-settling tank using fluent CFD software. Water Sci. Technol. 39 (4), 155–162.
Lakehal, D., Krebs, P., Krijgsman, J., Rodi, W., 1999. Computing shear flow and sludge blanket in secondary clarifiers. J. Hydraul. Eng. 125 (3), 253–262.
Larsen, P., 1977. On the Hydraulics of Rectangular Settling Basins: Experimental and Theoretical Studies. Department of Water Resources Engineering, Lund Institute of Technology, University of Lund.
Li, B., Stenstrom, M.K., 2014. Research advances and challenges in one-dimensional modeling of secondary settling tanks–a critical review. Water Res. 65, 40–63.
Lyn, D., Stamou, A., Rodi, W., 1992. Density currents and shear-induced flocculation in sedimentation tanks. J. Hydraul. Eng. 118 (6), 849–867.
Parker, D., Butler, R., Finger, R., Fisher, R., Fox, W., Kido, W., Merrill, S., Newman, G., Pope, R., Slapper, J., 1996. Design and operations experience with flocculator-clarifiers in large plants. Water Sci. Technol. 33 (12), 163–170.
Parker, D., Stenquist, R., 1986. Flocculator-clarifier performance. J. Water Pollut. Control Fed. 53 (3), 214–219.
Parker, D.S., 1983. Assessment of secondary clarification design concepts. J. Water Pollut. Control Fed. 55 (4), 349–359.
Patziger, M., 2016. Computational fluid dynamics investigation of shallow circular secondary settling tanks: inlet geometry and performance indicators. Chem. Eng. Res. Des. 112, 122–131.
Patziger, M., Gunthert, F.W., Jardin, N., Kainz, H., Londong, J., 2016. On the design and operation of primary settling tanks in state of the art wastewater treatment and water resources recovery. Water Sci. Technol. 74 (9), 2060–2067.
Patziger, M., Kainz, H., Hunze, M., Jozsa, J., 2012. Influence of secondary settling tank performance on suspended solids mass balance in activated sludge systems. Water Res. 46 (7), 2415–2424.
Patziger, M., Kiss, K., 2015. Analysis of suspended solids transport processes in primary settling tanks. Water Sci. Technol. 72 (1), 1–9.
Ramin, E., Wagner, D.S., Yde, L., Binning, P.J., Rasmussen, M.R., Mikkelsen, P.S., Plosz, B.G., 2014. A new settling velocity model to describe secondary sedimentation. Water Res. 66, 447–458.
Rodi, W., 1980. Turbulent Models and Their Application in Hydraulics—a State of the Art Review. International Association for Hydraulics Research, Delft.
Rodi, W., 1993. Turbulence Models and Their Application in Hydraulics. CRC Press.
Stamou, A., Adams, E., Rodi, W., 1989. Numerical modeling of flow and settling in primary rectangular clarifiers. J. Hydraul. Res. 27 (5), 665–682.
Stamou, A.I., Theodoridis, G., Xanthopoulos, K., 2009. Design of secondary settling tanks using a CFD model. J. Environ. Eng. 135 (7), 551–561.
Takács, I., Patry, G.G., Nolasco, D., 1991. A dynamic model of the clarification-thickening process. Water Res. 25 (10), 1263–1271.
Tamayol, A., Firoozabadi, B., Ahmadi, G., 2008. Effects of inlet position and baffle configuration on hydraulic performance of primary settling tanks. J. Hydraul. Eng. 134 (7), 1004–1009.
Tamayol, A., Firoozabadi, B., Ashjari, M., 2009. Hydrodynamics of secondary settling tanks and increasing their performance using baffles. J. Environ. Eng. 136 (1), 32–39.
Tarpagkou, R., Pantokratoras, A., 2013. CFD methodology for sedimentation tanks: the effect of secondary phase on fluid phase using DPM coupled calculations. Appl. Math. Model. 37 (5), 3478–3494.
Vitasovic, Z.C., Zhou, S., McCorquodale, J.A., Lingren, K., 1997. Secondary clarifier analysis using data from the Clarifier Research Technical Committee protocol. Water Environ. Res. 69 (5), 999–1007.
Wahlberg, E.J., Keinath, T.M., 1988. Development of settling flux curves using SVI. J. Water Pollut. Control Fed. 60 (12), 2095–2100.
Wang, X., Yang, L., Sun, Y., Song, L., Zhang, M., Cao, Y., 2008. Three-dimensional simulation on the water flow field and suspended solids concentration in the rectangular sedimentation tank. J. Environ. Eng. 134 (11), 902–911.
Weiss, M., Plósz, B.G., Essemiani, K., Meinhold, J., 2007. Suction-lift sludge removal and non-Newtonian flow behaviour in circular secondary clarifiers: numerical modelling and measurements. J. Chem. Eng. 132 (1–3), 241–255.
Wells, S.A., LaLiberte, D.M., 1998. Modeling density currents in circular clarifiers. J. Fluid/Particle Sep. 11 (1), 48–54.
Xanthos, S., Ramalingam, K., Lipke, S., McKenna, B., Fillos, J., 2013. Implementation of CFD modeling in the performance assessment and optimization of secondary clarifiers: the PVSC case study. Water Sci. Technol. 68 (9), 1901–1913.
Zhou, S., McCorquodale, J.A., 1992a. Influence of skirt radius on performance of circular clarifier with density stratification. Int. J. Numer. Meth. Fluid. 14 (8), 919–934.
Zhou, S., McCorquodale, J.A., 1992b. Mathematical modelling of a circular clarifier. Can. J. Civ. Eng. 19 (3), 365–374.
Zhou, S., McCorquodale, J.A., 1992c. Modeling of rectangular settling tanks. J. Hydraul. Eng. 118 (10), 1391–1405.
Zhou, S., McCorquodale, J.A., Vitasovic, Z., 1992. Influences of density on circular clarifiers with baffles. J. Environ. Eng. 118 (6), 829–847.